Supplementary Information

In-situ Study of CdS/WO_3 and CdS/SnO_2 Heterostructures: Comparison of Photocatalytic Activity Behavior

Hyejin Yu,[a ‡] *Dung Thanh Hoang,*[b, ‡] *Hyun Sung Kim*[*,a], *Hangil Lee*[*,b]

[a] Department of Chemistry, Pukyong National University, Busan 48513, Republic of Korea

[b] Department of Chemistry, Sookmyung Women's University, Seoul 04310, Republic of Korea

Table of Contents

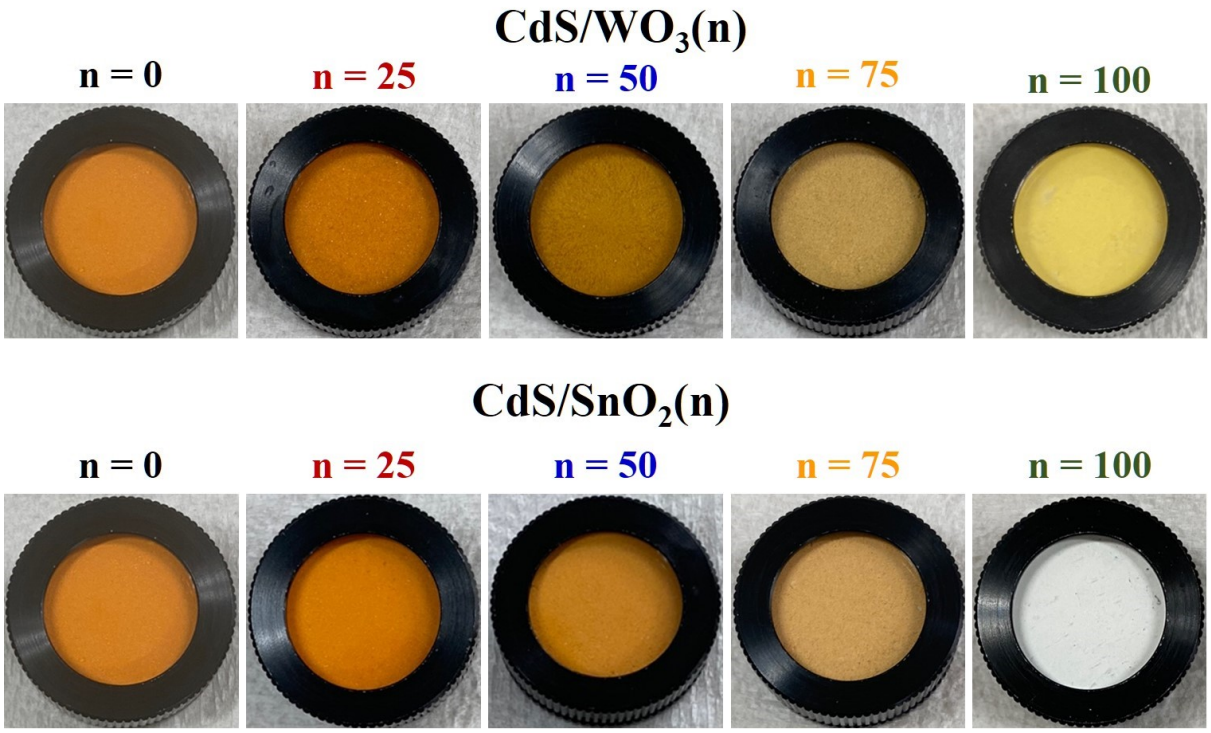

Figure S1. The samples of fabricated $CdS/WO_3(n)$ and $CdS/SnO_2(n)$ heterostructures (n = WO_3 or SnO_2 wt.%).

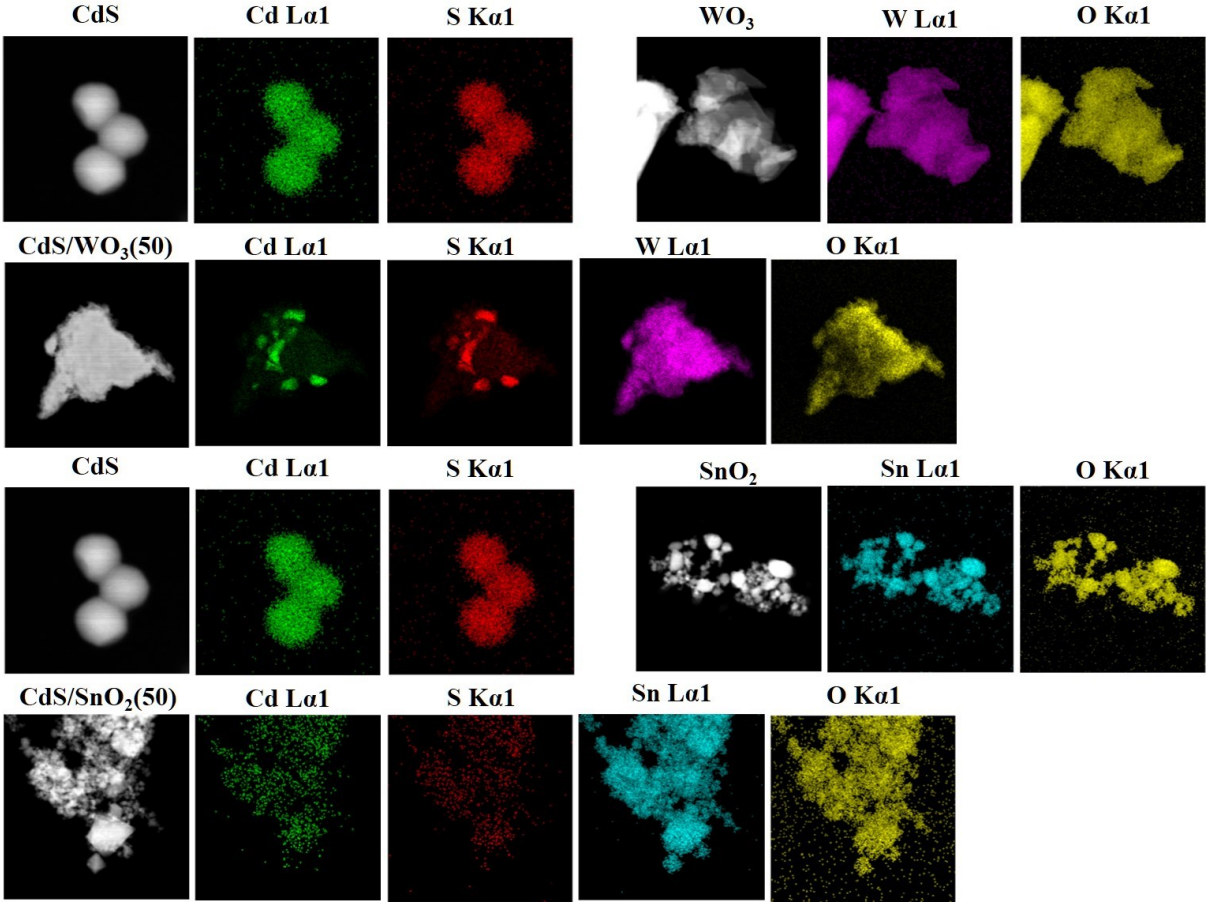

Figure S2. Energy-dispersive X-ray images of $CdS/WO_3(50)$ and $CdS/SnO_2(50)$ heterostructure systems.

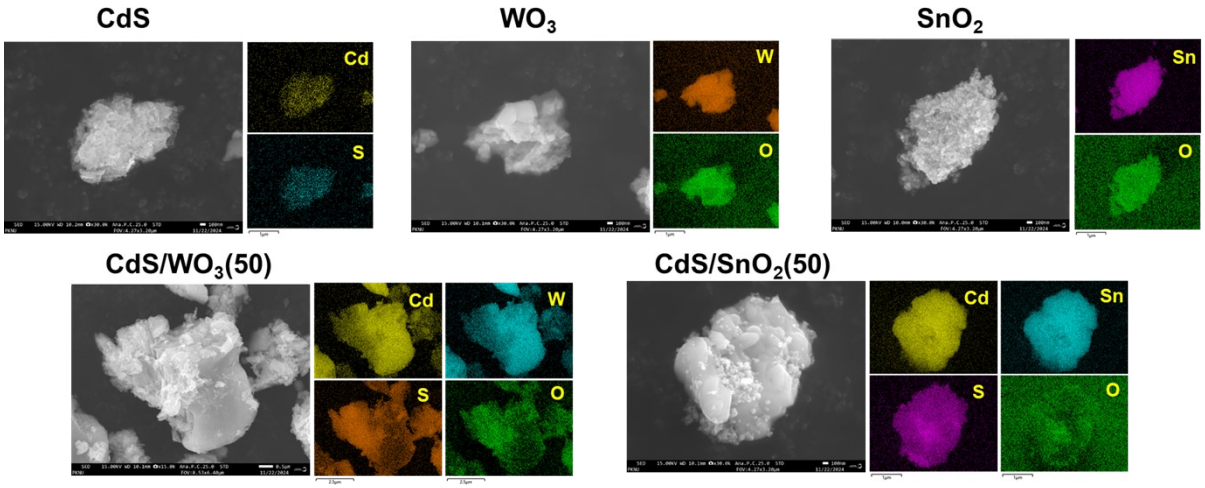

Figure S3. SEM Image and their EDS mapping of CdS, WO_3, SnO_2, CdS/WO_3(50), and CdS/SnO_2-(50).

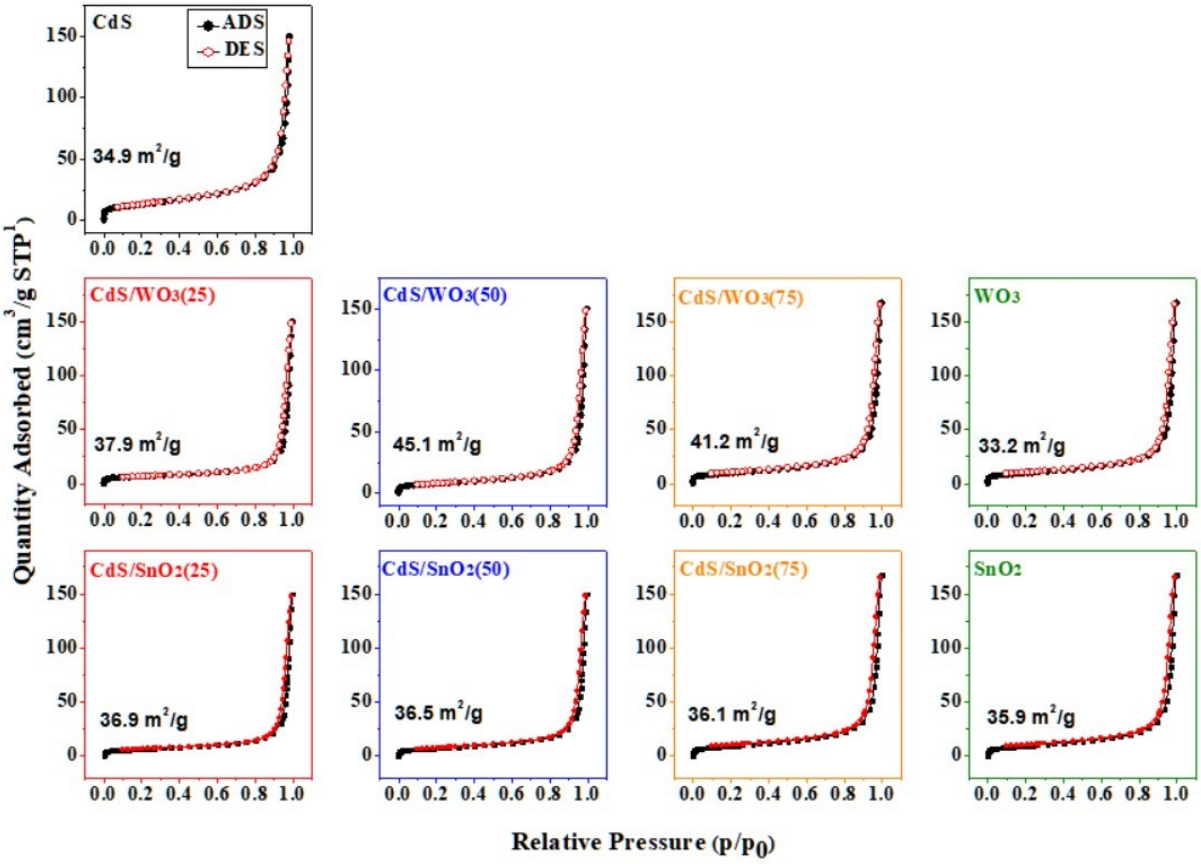

Figure S4. Brunauer-Emmett-Teller analysis of $CdS/WO_3(n)$ and $CdS/SnO_2(n)$ heterostructure systems (n = WO_3 or SnO_2 wt.%).

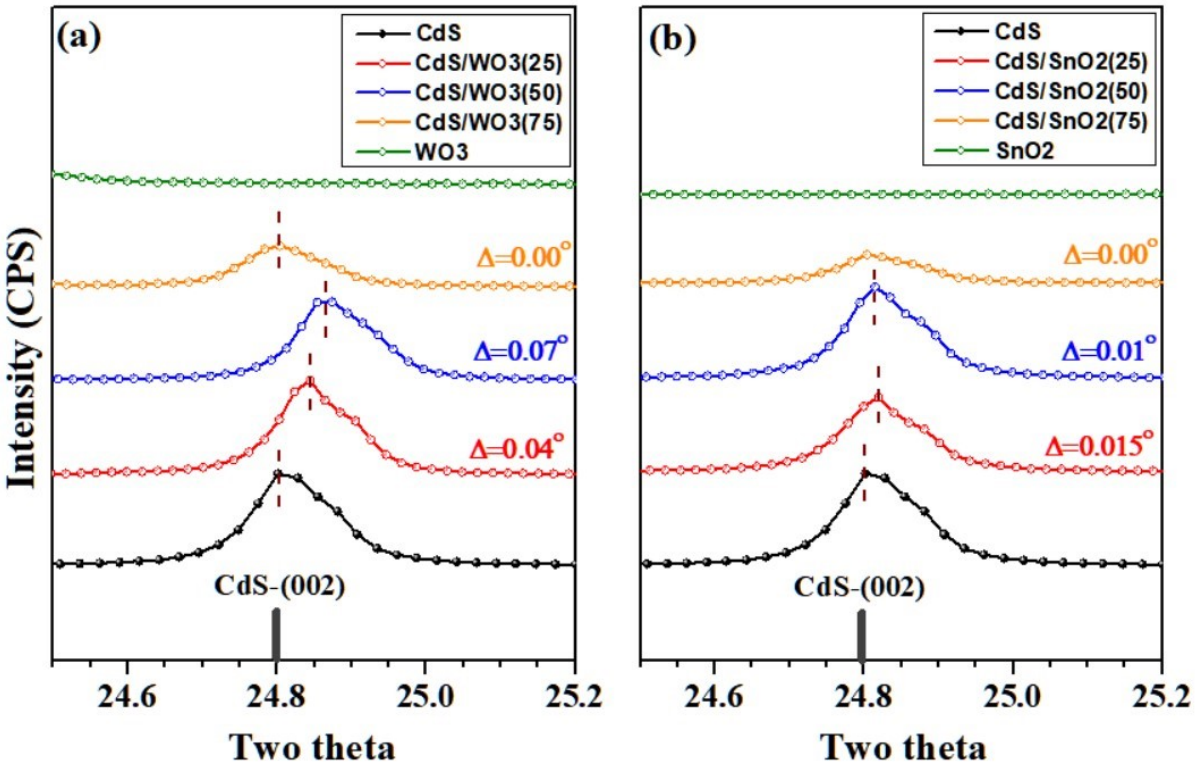

Figure S5. Small-angle XRD patterns of (a) $CdS/WO_3(n)$ and (b) $CdS/SnO_2(n)$ heterostructure systems (n = WO_3 or SnO_2 wt.%)..

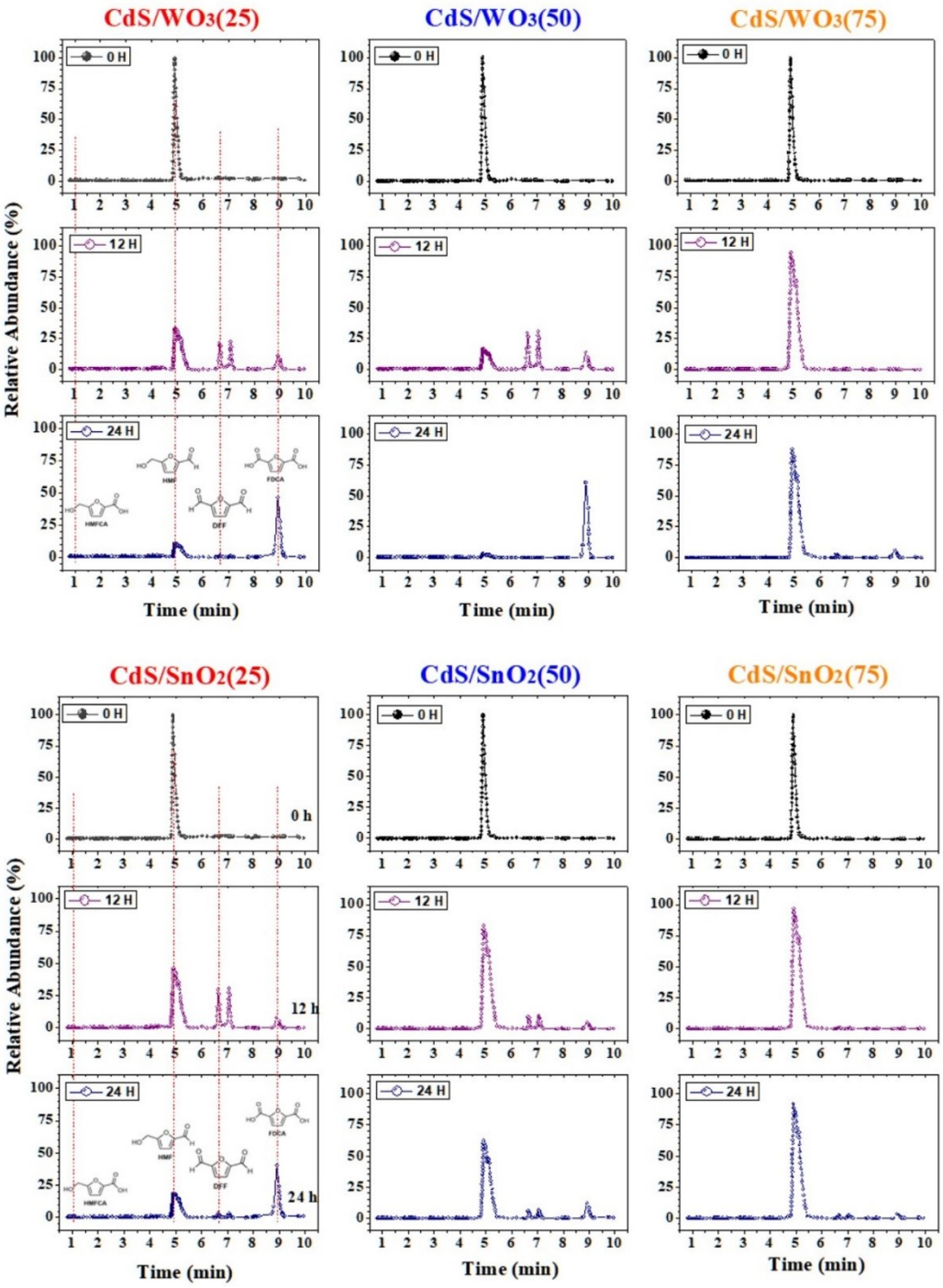

Figure S6. LC-MS results of $CdS/WO_3(n)$ and $CdS/SnO_2(n)$ heterostructure systems.

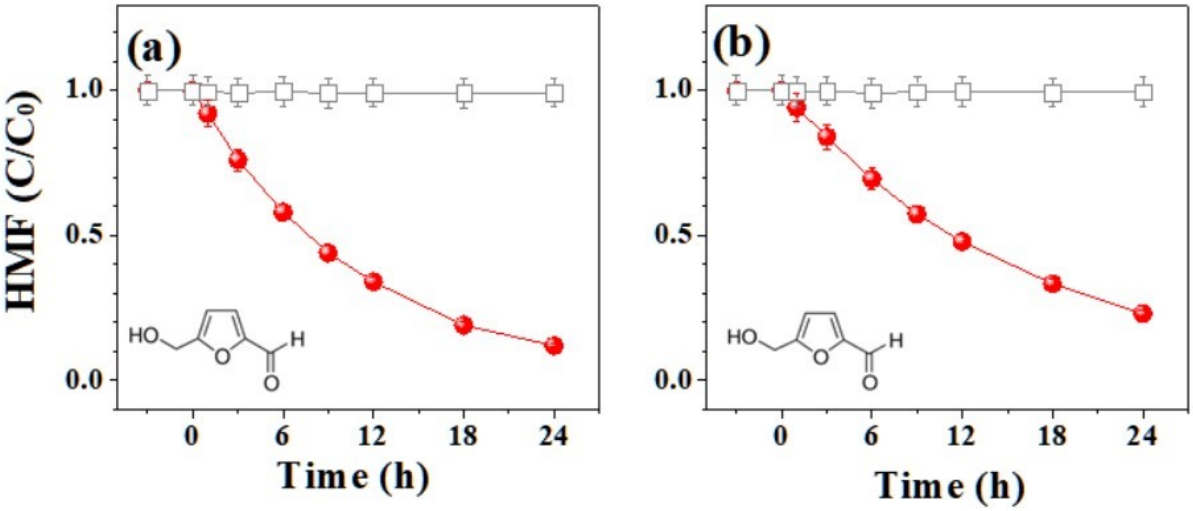

Figure S7. Photocatalytic degradation of HMF by (a) $CdS/WO_3(25)$ and (b) $CdS/SnO_2(25)$ heterostructures in the presence (grey color) and absence (red color) of DMPO as $\bullet O_2^-$scavenger.

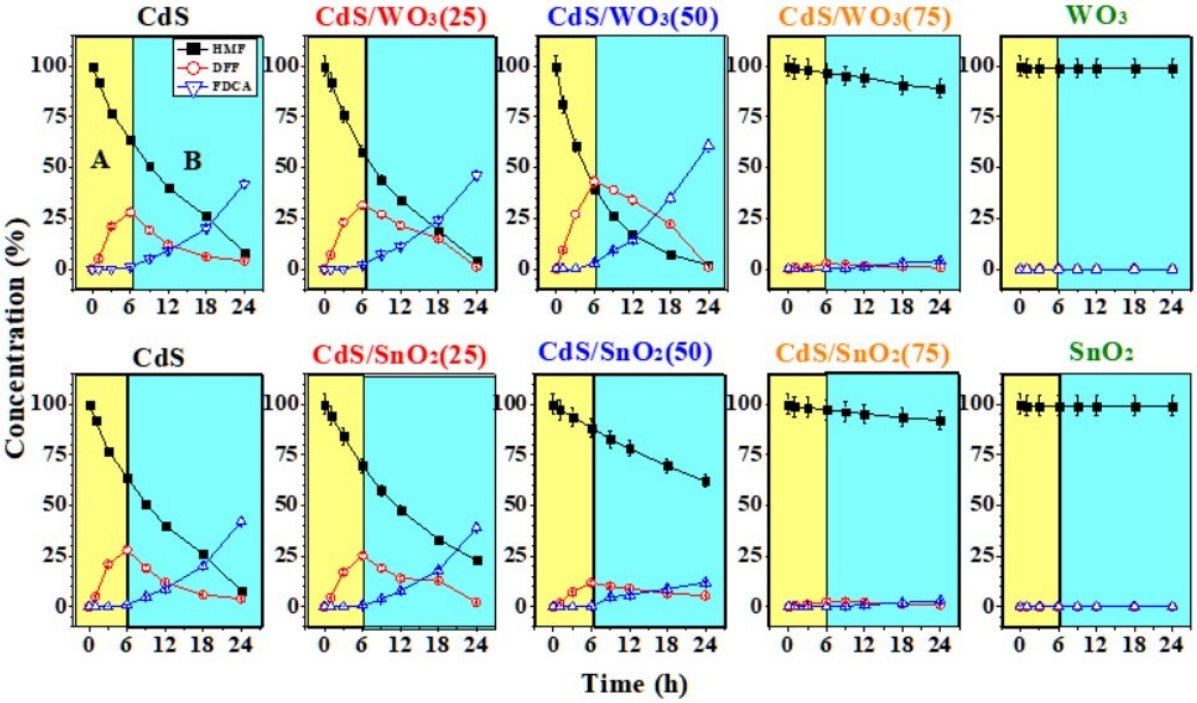

Figure S8. Product analysis through HPLC for selective oxidation from HMF to FDCA via DFF.

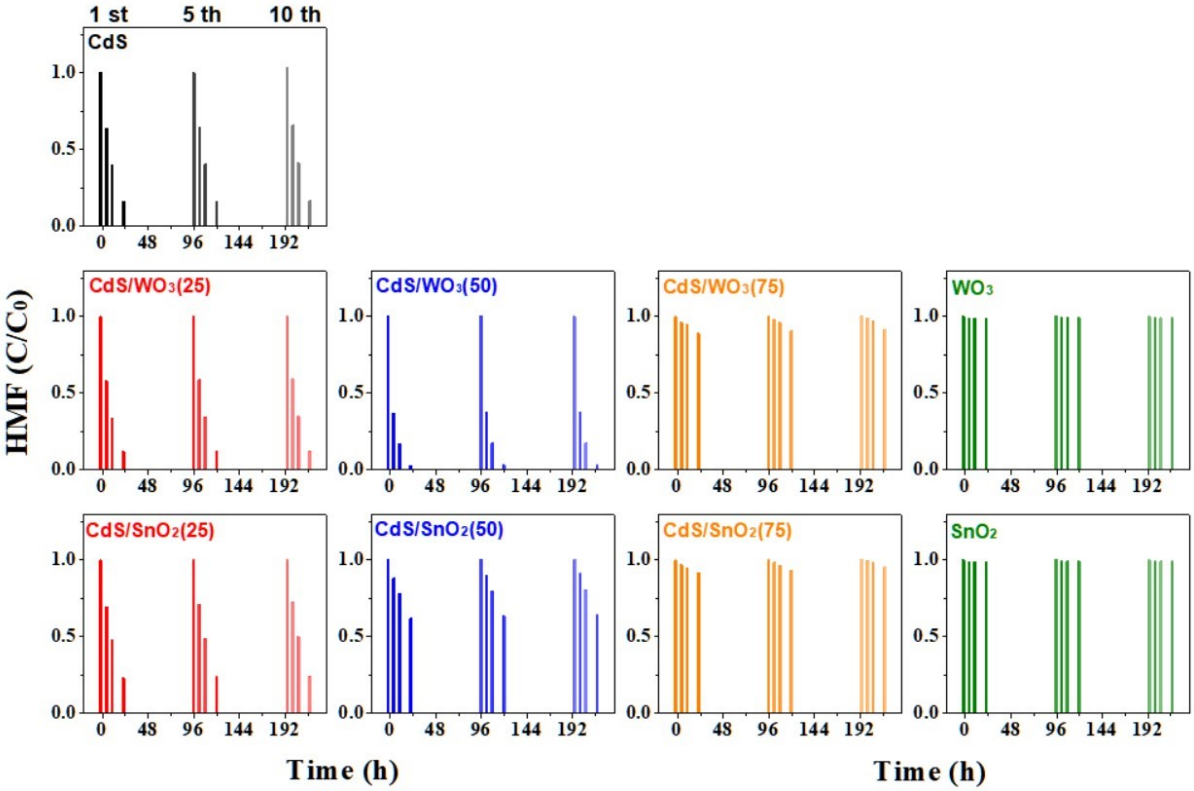

Figure S9. Photocatalytic HMF-decomposition degradation data over 10 cycles using $CdS/WO_3(n)$ and $CdS/SnO_2(n)$ heterostructure systems (n = WO_3 or SnO_2 wt.%).

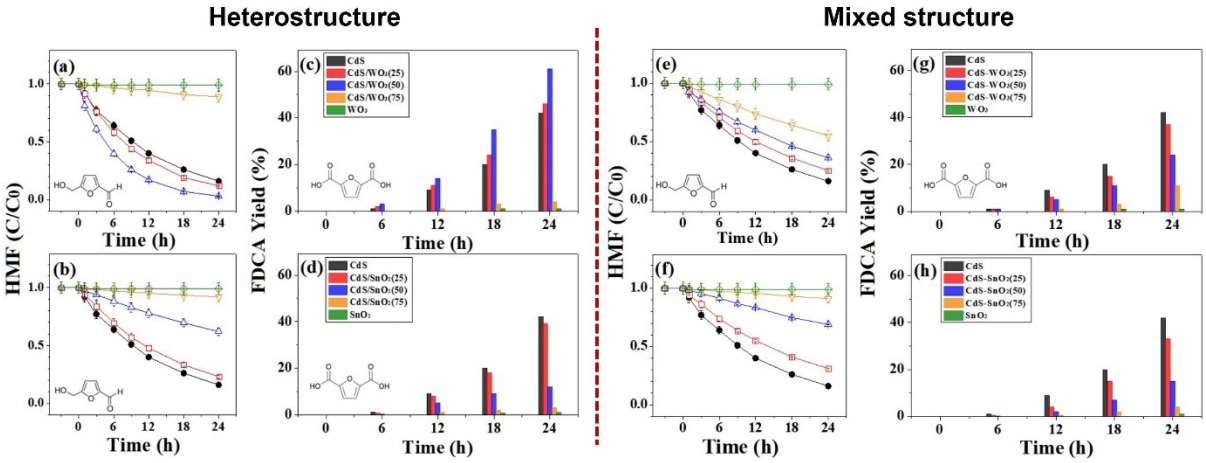

Figure S10. Comparison of Photocatalytic activities between heterostructure and physically mixed components. [Key: black—CdS; red—CdS/WO_3(25) and CdS/SnO_2(25) ; blue— CdS/WO_3(50) and CdS/SnO_2(50); orange— CdS/WO_3(75) and CdS/SnO_2(75); and green—WO_3 and SnO_2.].

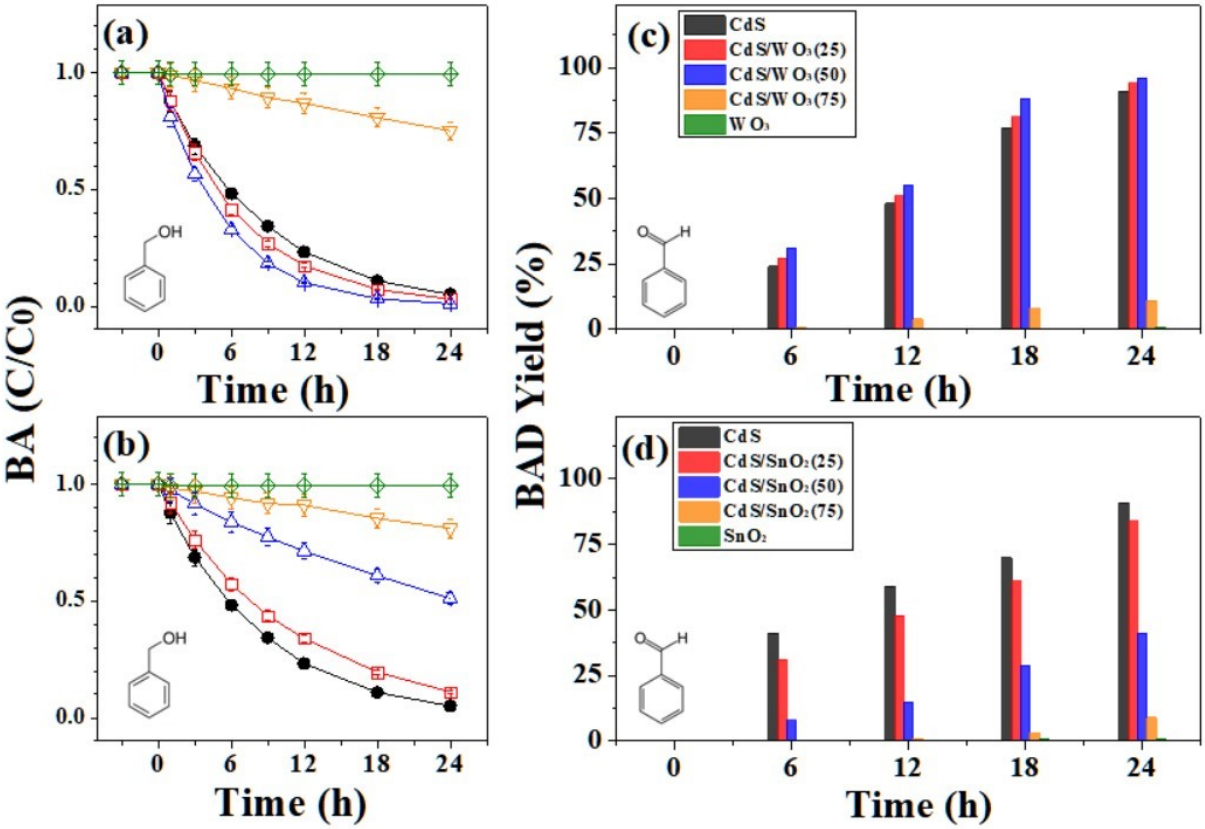

Figure S11. PCD activities of benzyl alcohol (BA) for (a) $CdS/WO_3(n)$ and (b) $CdS/SnO_2(n)$ heterostructures. [Key: black—CdS; red—$CdS/WO_3(25)$ and $CdS/SnO_2(25)$; blue— $CdS/WO_3(50)$ and $CdS/SnO_2(50)$; orange— $CdS/WO_3(75)$ and $CdS/SnO_2(75)$; and green—WO_3 and SnO_2.]. The yield of the end product, benzaldehyde (BAD), from BA for (c) $CdS/WO_3(n)$ and (d) $CdS/SnO_2(n)$ heterostructures with varying ratios, under at 445 nm irradiation over 24 h (n = WO_3 or SnO_2 wt.%).

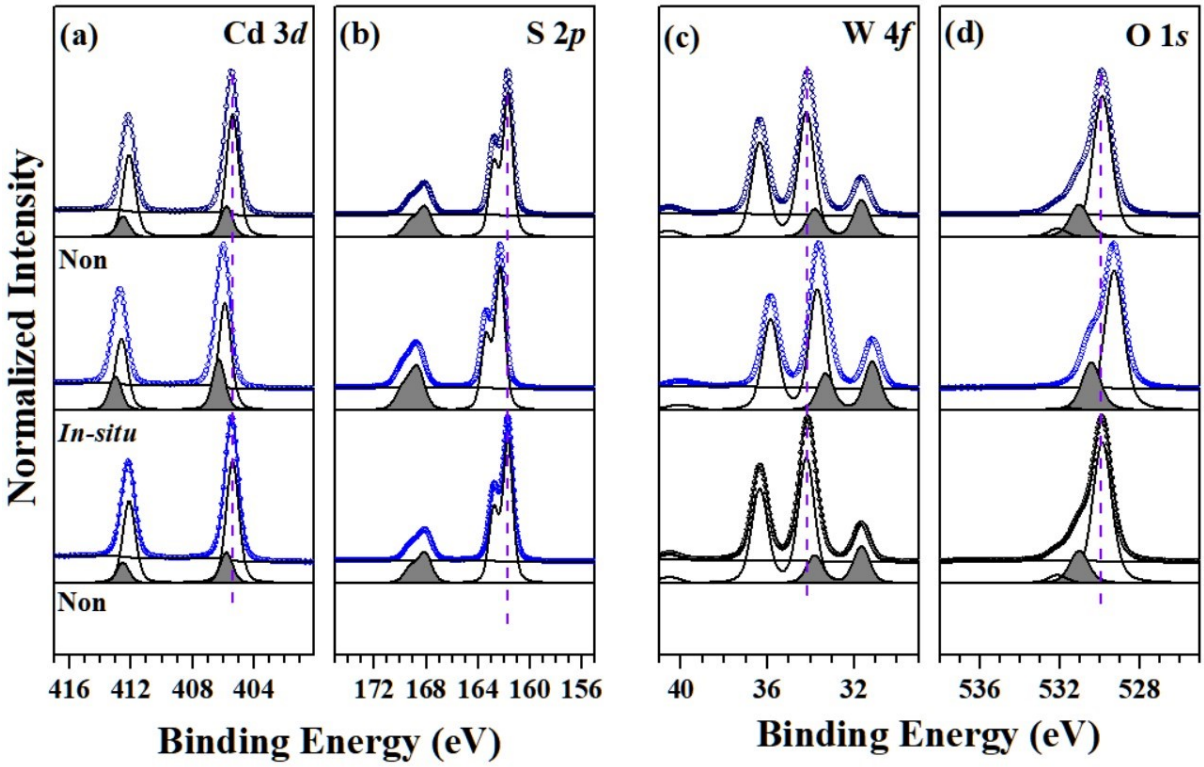

Figure S12. Confirmation of the photocatalytic reactivity of the CdS/WO_3(50) heterostructure system using *in-situ* XPS.

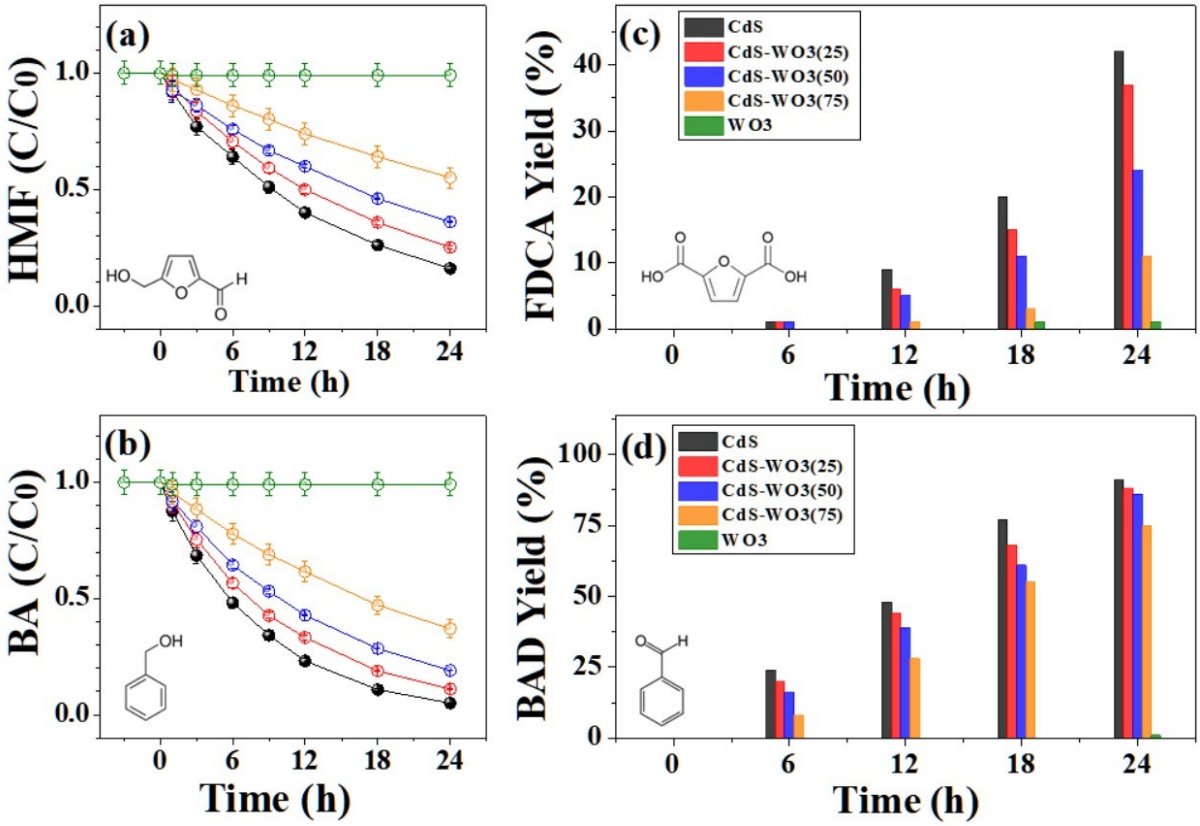

Figure S13. Photocatalytic conversion activities of (a) HMF and (b) BA for CdS–WO_3(n) mixed samples. Yield of the end product, (c) FDCA from HMF and (d) BAD from BA, for CdS–WO_3(n) mixed samples with varying ratios under 445 nm irradiation over 24 h. * The bar (–) indicates physical mixing between CdS and WO_3 NPs (n = WO_3 or SnO_2 wt.%).

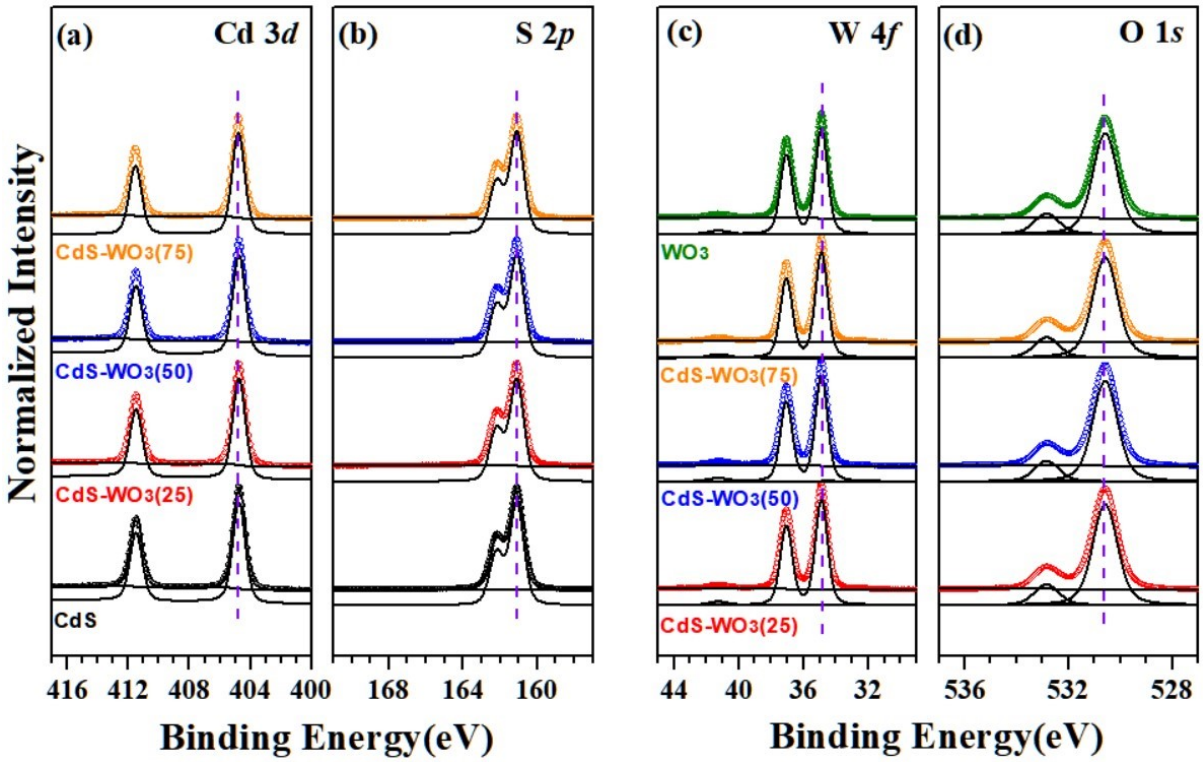

Figure S14. (a) Cd 3*d*, (b) S 2*p*, (c) W 4*f*, and (d) O 1*s* core-level X-ray photoelectron spectra of CdS–WO_3(n) mixed samples. Colors indicate the ratio between the two heterostructures: n = 0 (black), n = 25 (red), n = 50 (blue), n = 75 (orange), and n = 100 (olive). * The bar (–) indicates physical mixing between CdS and WO_3 NPs (n = WO_3 or SnO_2 wt.%).

Table S1. Specific surface area S_{BET} of $CdS/WO_3(n)$ and $CdS/SnO_2(n)$ heterostructures, as a function of ratio, using BET analysis (n = WO_3 or SnO_2 wt.%).

Samples	CdS	$CdS/WO_3(25)$	$CdS/WO_3(50)$	$CdS/WO_3(75)$	WO_3
S_{BET} (m^2/g)	34.9	37.9	**45.1**	41.2	33.2
Samples	CdS	$CdS/SnO_2(25)$	$CdS/SnO_2(50)$	$CdS/SnO_2(75)$	SnO_2
S_{BET} (m^2/g)	**34.9**	36.9	36.5	36.1	35.9